Inorganic Chemistry

ARTICLE

pubs.acs.org/IC

Revised Ionic Radii of Lanthanoid(III) Ions in Aqueous Solution

Paola D'Angelo,*[,†] Andrea Zitolo,[†] Valentina Migliorati,[†] Giovanni Chillemi,[‡] Magali Duvail,[§] Pierre Vitorge,[§,∥] Sacha Abadie,[†,§] and Riccardo Spezia[§]

[†]Department of Chemistry, University of Rome "La Sapienza", P. le A. Moro 5, 00185 Roma, Italy

[‡]CASPUR, Inter-University Consortium for Supercomputing in Research, via dei Tizii 6b, 00185 Roma, Italy

[§]Laboratoire Analyse et Modelisation pour la Biologie et l'Environnement, UMR 8587 CNRS-CEA-UEVE, Université d'Evry Val d'Essonne, Bd F. Mitterrand, 91025 Evry Cedex, France

[∥]Laboratoire de Speciation des Radionucleides et des Molecules, CEA, DEN, F-91191 Gif-sur-Yvette, France

Supporting Information

ABSTRACT: A new set of ionic radii in aqueous solution has been derived for lanthanoid(III) cations starting from a very accurate experimental determination of the ion−water distances obtained from extended X-ray absorption fine structure (EXAFS) data. At variance with previous results, a very regular trend has been obtained, as expected for this series of elements. A general procedure to compute ionic radii in solution by combining the EXAFS technique and molecular dynamics (MD) structural data has been developed. This method can be applied to other ions allowing one to determine ionic radii in solution with an accuracy comparable to that of the Shannon crystal ionic radii.

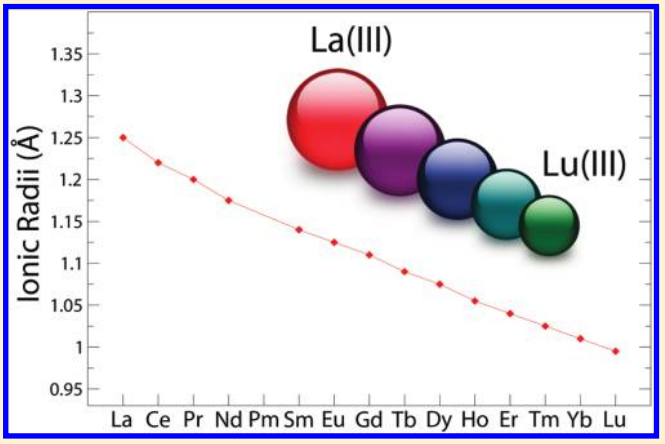

1. INTRODUCTION

A full characterization of electrolyte solutions in terms of their thermodynamic, structural, transport, and spectroscopic properties requires the knowledge of the ability of the solvent to approach a given ion. This ability is strictly dependent on the "ionic radii" of the ions. In 1976, Shannon published a comprehensive list of ionic radii, still in use nowadays,[1] based on inorganic structures with highly symmetric lattices. Different sets of ionic radii were proposed depending on the ion coordination number starting from bond distances found in X-ray-determined structures of halides and chalcogenides, and a strong correlation between the coordination numbers and the ionic radii was observed.

In many cases the "crystal ionic radii" are employed to derive ion properties in liquid phase and in electrolyte solutions, even if it is not immediately obvious that the radii of ions determined in crystalline compounds can be extended to ions in liquid solutions. In particular, it is expected that a close relation between the coordination number of an ion and its size exists also in the liquid phase. As a consequence, the correct solvation number should be taken into account to evaluate ionic radii in solution. Moreover, packing effects are expected to have an influence on the bond distance distribution, and use of experimental distances obtained from solution studies is highly desirable. These considerations have stimulated some authors to develop ionic radii in solution starting from experimental determinations of distances between the ions and the surrounding solvent molecules.[2,3]

The coordination chemistry of lanthanoid(III), Ln(III), ions follows a more regular pattern than any other series in the periodic table and this makes these elements ideal for comparative studies. Questions about the change of structure of the first hydration shell across the lanthanoid series are still at the center of recent research works.[4−7] A number of investigations were carried out on this topic from both an experimental[4,5,8−13] and theoretical[6,7,14−26] point of view, and a consensus did emerge from the experimental data in aqueous solution that a change of the coordination number from nine to eight takes place in the middle of the series.[10] Recently, a thorough X-ray absorption analysis has shown that all of the Ln(III) hydration complexes in aqueous solution retain a tricapped trigonal prism (TTP) geometry, in which the bonding of the capping water molecules varies along the series.[5,13] A similar behavior was found in a recent molecular dynamics (MD) study of the whole series.[7,27,28] From these simulations, based on a pair interaction potential with polarization, it was confirmed that the coordination number

Received: February 7, 2011
Published: April 15, 2011

changes smoothly across the series from 9 to 8. The 9-fold tricapped trigonal prism geometry, typical of light Ln(III) ions, is progressively destabilized across the series since the interaction of one of the equatorial water molecules becomes weaker and first to second shell exchanges increase reaching a maximum in the middle of the series. Then, the 8-fold geometry becomes more stable, always in a dynamical interchange with the 9-fold geometry, and it is basically the unique hydration structure at the end of the series.

Clearly, the reliability of the ionic radii in solution is strictly dependent on the accuracy of the ion−solvent distances used in their evaluation. While the determination of bond distances is quite straightforward for crystalline samples, the characterization of structures in solution is more elusive and very difficult to obtain from the standard experimental techniques.[5] With regards to structural studies of ion coordination in dilute solutions extended X-ray absorption fine structure (EXAFS) spectroscopy is the structural probe of choice; because of its intrinsic chemical specificity and short-range sensitivity this technique measures a less complex correlation function as compared to X-ray and neutron diffraction, that contains very accurate structural information on the first coordination shell distance. However, a proper extraction of the structural parameters from the EXAFS experimental signal relies on the use of reliable starting models that can be obtained from MD simulations.

This work aims at proposing a new improved set of ionic radii for lanthanoid(III) cations in aqueous solution starting from a very accurate experimental determination of the Ln(III)-water distances obtained from EXAFS data in combination with state of the art MD simulations. The present study shows that the combination of EXAFS spectroscopy and MD calculations allows one to enhance the reliability of the structural information obtained on the ion−solvent distances in solution, thus making the combination of these techniques powerful for the derivation of improved ionic radii for all ions in solution.

2. EXPERIMENTAL SECTION

2.1. X-ray Absorption Measurements. Aqueous solutions of the Ln(III) ions were made by dissolving a weighed amount of hydrated trifluoromethanesulfonates $[Ln(H_2O)_n](CF_3SO_3)_3$ (Ln = La, Pr, Nd, Sm, Eu, Gd, Tb, Dy, Ho, Er, Tm, Yb, and Lu) in freshly distilled water. The concentration of the samples was 0.2 M, and the solutions were acidified to about pH = 1 by adding trifluoromethanesulfonic acid to avoid hydrolysis. The K-edge spectra were collected at ESRF, on the bending magnet X-ray-absorption spectroscopy beamline BM29,[29] in transmission geometry. The storage ring was operating in 16-bunch mode with a typical current of 80 mA after refill. The spectra were collected by using a Si(511) double-crystal monochromator with the second crystal detuned by 20% for harmonic rejection. The aqueous solutions were kept in cells with Kapton film windows and Teflon spacers ranging from 2 to 3 cm depending on the sample. Internal energy calibration was made when possible with a foil of the corresponding lanthanoid metal.

2.2. EXAFS Data Analysis. The EXAFS data analysis has been performed using the GNXAS program, which has proven to give reliable structural information also in the high energy domain.[30] K-edge spectra have been used as it has been shown that for lanthanoid ions although the core hole width is five time larger at the K-edge than at the L_3 one, the analysis of the K-edge EXAFS data provides more accurate structural results.[30] This is due both to the smaller influence of the double-electron excitations that strongly affect the L_3 edges, and to the wider k-range available which extends more than a factor of 2 over the L_3-edge of the lighter lanthanoids. In addition, in the case of disordered systems such as aqueous solutions, high frequency components are strongly damped in the spectra, and the structural information content of the K-edges is the same as the L_3 ones. A thorough description of the theoretical framework for the multiple scattering analysis can be found in refs 31,32. Phase shifts have been calculated for each system starting from one of the MD configurations, by using muffin-tin potentials and advanced models for the exchange-correlation self-energy (Hedin−Lundqvist). Inelastic losses of the photoelectron in the final state have been accounted for intrinsically by a complex potential. The GNXAS method is based on the theoretical calculation of the EXAFS signal and a subsequent refinement of the structural parameters. In the case of ionic solutions the radial distribution functions associated with the solvent molecules are not Gaussian in form and the neglect of this asymmetry in EXAFS data analysis leads to unreliable results: interatomic distances and coordination numbers are underestimated. This is also true for lanthanoid(III) aqueous solutions where the first hydration shell has a TTP geometry that becomes more and more distorted along the series.[5]

In the first step of the analysis the Ln(III)-oxygen first coordination shells have been modeled with gamma-like distribution curves with mean distance R, standard deviation σ, and asymmetry index (third cumulant divided by σ^3) $\beta = 2p^{-1/2}$ that can be gradually varied in a wide range. The general expression is

$$g(r) = N\frac{p^{1/2}}{\sigma\Gamma(p)}\left[p + \left(\frac{r-R}{\sigma}\right)p^{1/2}\right]^{p-1} \exp\left[-p - \left(\frac{r-R}{\sigma}\right)p^{1/2}\right] \quad (1)$$

where $\Gamma(p)$ is the Euler's Gamma function for the parameter p, and N is the coordination number providing the correct normalization. Note that the R values are the average distances of the distributions that are shifted toward larger values with respect to the maximum of the $g(r)$'s because of the asymmetry.

Least-squares fits of the EXAFS raw experimental data are performed to optimize the structural parameters, and two additional non structural parameters, namely, E_0 (core ionization threshold energy) and S_0^2.

The EXAFS data analysis of the whole series of Ln(III) ions in aqueous solution has been performed using a single-shell model to analyze the K-edge spectra. The minimizations were performed in the range k = 2.4−15.0 Å^{-1}, and the results are shown in Figure 1, for Ce(III), Sm(III), and Tm(III), as an example. In the upper panels of Figure 1 the total theoretical signals comprising both the short and the long distances of the tricapped trigonal prism are compared with the experimental data for the three elements. Note that the theoretical models contain both the ion-oxygen and the ion-hydrogen signals as the ion-hydrogen interactions have been found to provide a detectable contribution to the EXAFS spectra of lanthanoid ions in aqueous solutions.[5,30] The agreement between the experimental and the theoretical spectra is excellent, and this is also evident from the corresponding k^2 weighted Fourier transform (FT) spectra shown in the lower panels of Figure 1. The FT spectra were calculated with no phase shift correction applied, in the k-range 3.4−13.5 Å^{-1}. The Ln−O structural parameters obtained from this analysis for the entire series are reported in Table 1.

Recent investigations carried out on aqueous solutions of 3d metal ions[30,33−35] and halides[36,37] have shown that the EXAFS technique can be profitably used to assess the reliability of structural results obtained from computer simulations. Rather than using the usual discrete form of the EXAFS equation, in this case the signal is modeled as a function of the radial distribution function $g(r)$ as

$$\chi(k) = \int_0^\infty dr\, 4\pi\rho r^2 g(r)\, A(k,r)\, \sin[2kr + \phi(k,r)] \quad (2)$$

where $A(k,r)$ and $\phi(k,r)$ are the amplitude and phase functions,

dx.doi.org/10.1021/ic200260r |Inorg. Chem. 2011, 50, 4572–4579

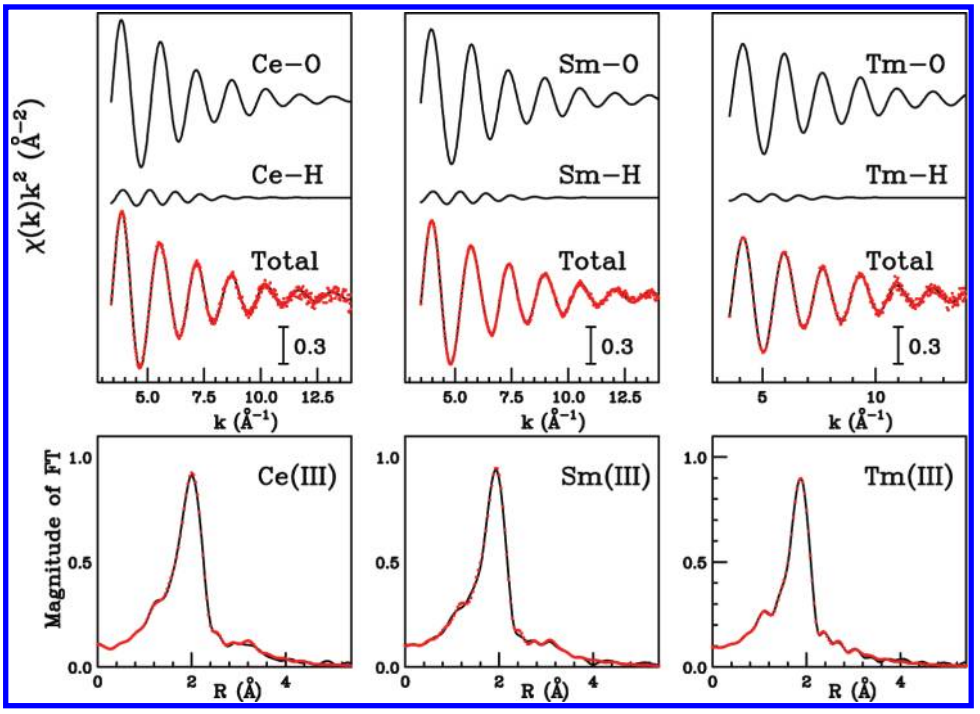

Figure 1. Upper panels: fits of the K-edge EXAFS spectra of Ce(III), Sm(III), and Tm(III) in aqueous solution (red dotted line are the experimental data, black full line are the theoretical models) by using a single asymmetric shell. Lower panels: nonphase-shift-corrected Fourier transforms of the experimental data (red dotted line) and of the total theoretical signals (black full line).

Table 1. Ln−O First Shell Structural Parameters of Ln(III) Ions in Aqueous Solution Determined from the EXAFS Analysis [a]

	N	R (Å)	σ^2 (Å^2)	β
La−O	9.1(0.5)	2.600(0.007)	0.010(0.001)	0.47
Ce−O	9.0(0.5)	2.570(0.007)	0.010(0.001)	0.48
Pr−O	9.0(0.5)	2.550(0.007)	0.011(0.001)	0.49
Nd−O	9.0(0.5)	2.525(0.007)	0.010(0.001)	0.50
Sm−O	9.0(0.5)	2.490(0.007)	0.010(0.001)	0.52
Eu−O	9.0(0.5)	2.470(0.007)	0.009(0.001)	0.55
Gd−O	9.0(0.5)	2.455(0.0 08)	0.009(0.001)	0.59
Tb−O	9.0(0.5)	2.440(0.008)	0.008(0.001)	0.61
Dy−O	9.0(0.5)	2.425(0.008)	0.008(0.001)	0.64
Ho−O	8.9(0.5)	2.405(0.007)	0.008(0.001)	0.65
Er−O	8.9(0.5)	2.390(0.007)	0.007(0.001)	0.65
Tm−O	8.8(0.5)	2.375(0.008)	0.007(0.001)	0.52
Yb−O	8.7(0.5)	2.360(0.008)	0.008(0.001)	0.47
Lu−O	8.2(0.5)	2.345(0.008)	0.007(0.001)	0.44

[a] N is the coordination number, R is the average distance of the Ln−O distribution, σ^2 is the Debye−Waller factor, and β is the asymmetry parameter.

respectively, and ρ is the density of the scattering atoms. $\chi(k)$ theoretical signals can be calculated by introducing in eq 2 the model $g(r)$'s obtained from molecular dynamics simulations, and the comparison between the theoretical and experimental $\chi(k)$ signals allows the reliability of the $g(r)$'s, and consequently of the theoretical scheme used in the simulations, to be checked.

In the second step of the analysis both the Ln(III)-O and Ln(III)-H $g(r)$'s obtained from the different MD simulations have been used to calculate the single scattering first shell $\chi(k)_{MD}$ theoretical signals. The structural parameters derived from the MD simulations were kept fixed during the EXAFS analysis. In this way, the first hydration shell structure obtained from the simulations can be directly compared with experimental data, and the validity of the theoretical framework used in the simulations can be assessed. The results of this analysis will be described in the following.

2.3. Molecular Dynamics Simulations. MD simulations of Ln(III) ions in aqueous solution have been performed using the polarizable potential developed by some of us[6,27] where the non-electrostatic parameters between the Ln(III) ions and water depend on ionic radii. The total interaction potential is modeled as a sum of different terms

$$V_{tot} = V_{elec} + V^{LJ}_{O-O} + V_{Ln-O} \quad (3)$$

where V_{elec} is the electrostatic energy term composed by a Coulomb and a polarization term following the Thole's induced dipole model.[38] Also the atomic polarizability directly enters in the polarization part of the electrostatic energy term, and we used the values reported in ref 39. V^{LJ}_{O-O} is the 12−6 Lennard-Jones potential describing the O−O interaction. For water−water interaction, we used the TIP3P water model including polarization.[6,40] V_{Ln-O} accounts for the *non electrostatic* Ln−O interaction potential. We employed the following pair potential:

$$V^{Buck6}_{ij} = A_{ij} \exp(-B_{ij} r_{ij}) - \frac{C_{ij}}{r^6_{ij}} \quad (4)$$

where the parameters originally obtained for La(III) were adapted to all the atoms in the series considering changing of ionic radii across the series.[6,27]

In our previous works[6,27] we considered two sets of Shannon radii[1] that were obtained from solid phase experiments and are environment dependent: 9-fold radii and 8-fold radii, called hereafter $Ln^{III}_{(9)}$ and $Ln^{III}_{(8)}$, respectively. Here, as we will discuss in the following, we have derived a new set of ionic radii from EXAFS data, called hereafter Ln^{III}_{new}. The new set of parameters are listed in Supporting Information,

dx.doi.org/10.1021/ic200260r |*Inorg. Chem.* 2011, 50, 4572–4579

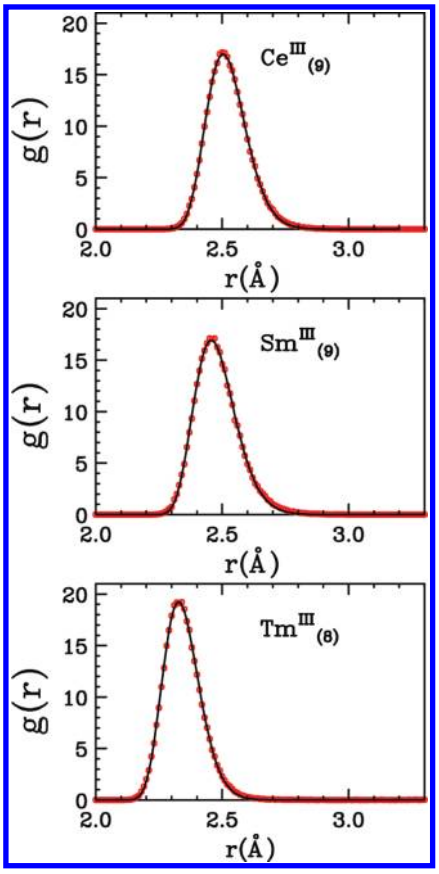

Figure 2. Ce(III), Sm(III), and Tm(III) Ln−O $g(r)$'s obtained from MD simulations using 9-fold or 8-fold Shannon radii (dotted red line) and corresponding gamma-like asymmetric peaks obtained from the fitting procedure (solid black line).

Table S1. Note that this procedure to construct a potential which systematically depends on lanthanoid radius is very similar to what was done by Madden and co-workers in the case of molten salts.[41,42]

MD simulations of the hydrated Ln(III) ions have been carried out in the microcanonical *NVE* ensemble with our own developed CLMD code MDVRY,[43] using the extended Lagrangian method to obtain atomic induced dipoles during the dynamics.[44] CLMD simulations were performed for one Ln(III) ion and 216 rigid water molecules in a cubic box at room temperature. Periodic boundary conditions were applied to the simulation box. Long-range interactions were calculated by using Smooth Particle Mesh Ewald (SPME) method.[45] Simulations were performed using a Velocity-Verlet-Based Multiple Time Scale (MTS) with a time step of 1 fs. Each system was equilibrated at 298 K for 2 ps. Production runs were subsequently collected for 3 ns. All other simulations details are the same as reported previously.[6,7,27,46]

The structural properties of the lanthanoid aqueous solutions obtained from the simulations are described in terms of radial distribution functions, $g_{Ln-O}(r)$ and $g_{Ln-H}(r)$:

$$g_{AB}(r) = \frac{\langle \rho_B(r) \rangle}{\langle \rho_B \rangle_{local}} = \frac{1}{N_A \langle \rho_B \rangle_{local}} \sum_{i=1}^{N_A} \sum_{j=1}^{N_B} \frac{\delta(r_{ij} - r)}{4\pi r^2} \quad (5)$$

where $\langle \rho_B(r) \rangle$ is the particle density of type B at distance r around type A, and $\langle \rho_B \rangle_{local}$ is the particle density of type B averaged over all spheres around particle A with radius r_{max}. To directly compare the MD and EXAFS structural results the Ln−O and Ln−H $g(r)$'s are modeled with the gamma-like peaks of eq 1 whose parameters are fitted to the MD distributions. The Ce(III), Sm(III), and Tm(III) Ln−O $g(r)$'s obtained from the MD simulations are shown in Figure 2 as an example, together with the asymmetric peaks obtained from the fitting procedure. The structural parameters obtained from the fitting of the MD $g(r)$'s are collected in Table 3 and Supporting Information, Tables S2−S4 for the entire series. These values can be directly compared with the EXAFS results of Table 1.

3. RESULTS AND DISCUSSION

3.1. Determination of Ionic Radii from EXAFS Data. As previously mentioned ionic radii determined in the crystalline phase are often used to derive properties of liquid systems. This procedure has been recently employed to develop Ln−O interaction potentials used in polarized MD simulations.[6,7,27,46] However, when one seeks to investigate liquid systems, the use of ionic radii specifically developed for solutions is preferable.

A thorough investigation aimed at determining ionic radii in aqueous solution has been carried out by Marcus.[2] In this work the ionic radii R_{ion} were derived starting from experimental ion−water internuclear distances:

$$R_{ion} = d_{ion-water} - R_{water} \quad (6)$$

where R_{water} is a distance that characterizes the "radius" of a water molecule and $d_{ion-water}$ is an appropriate value that defines the ion−water distance and is strictly dependent on the shape of the ion−water $g(r)$'s.

Application of eq 6 needs a proper choice of the R_{water} value and different strategies have been adopted in the literature. In the original work of Marcus[2] one uniform value of 1.39 Å was used for all ions, while in a subsequent study it was shown that the alkali metal cations and halogen anions have different R_{water} values.[47] David et al.[48] determined R_{water} by subtracting the Shannon ionic radii from the $d_{ion-water}$ distances, and found that the radius of the water molecule varies between 1.34 and 1.43 Å, depending on the charge of the ion. A similar procedure was carried out by Heyrovska[3] but the R_{water} values were much shorter for monovalent or divalent cations (0.64, 0.80, 1.10 Å), while a value of 1.37 Å was determined for trivalent cations in agreement with Marcus[2] and David et al.[48]

Another important issue for the derivation of ionic radii in solution is the accuracy of the experimental ion−water distances adopted in the calculation. X-ray and neutron diffraction are the most widely used techniques for the investigation of ion solvation, but they often provide contradictory structural results.[49] In the past years EXAFS has proven to be the most suitable technique for the structural characterization of the ion first coordination shell. In the standard EXAFS analysis the coordination of the photoabsorber is usually defined, in the small disorder limit or harmonic approximation, by means of Gaussian shells. This is a valid approximation for solids and liquids in which a high degree of local order is preserved by covalent bonding or strong ion−ion interactions. In general, solutions are expected to possess moderate to large disorder, and the application of this procedure can produce significant errors in the determination of the structural parameters. However, by careful modeling of the assumed radial distribution functions, the final results of an EXAFS analysis of complex fluids can be very accurate. A method to analyze EXAFS spectra of liquid systems by fitting $g(r)$ models obtained from MD simulations has been successfully applied to the investigation of several aqueous and non-aqueous ionic solutions.[33,37,50−55] When MD simulations are not wide of the mark, the fitting process is similar to a minimization with

dx.doi.org/10.1021/ic200260r |*Inorg. Chem.* 2011, 50, 4572–4579

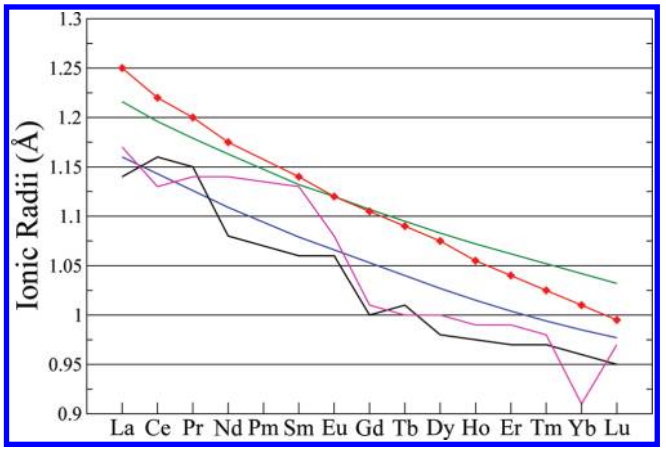

Figure 3. Ionic radii of Ln(III) in aqueous solution as determined by Marcus[2] (black line), by Heyrovska[3] (magenta line), in this work (red line) together with the Shannon 8-fold (blue line) and 9-fold (green line) crystal ionic radii.

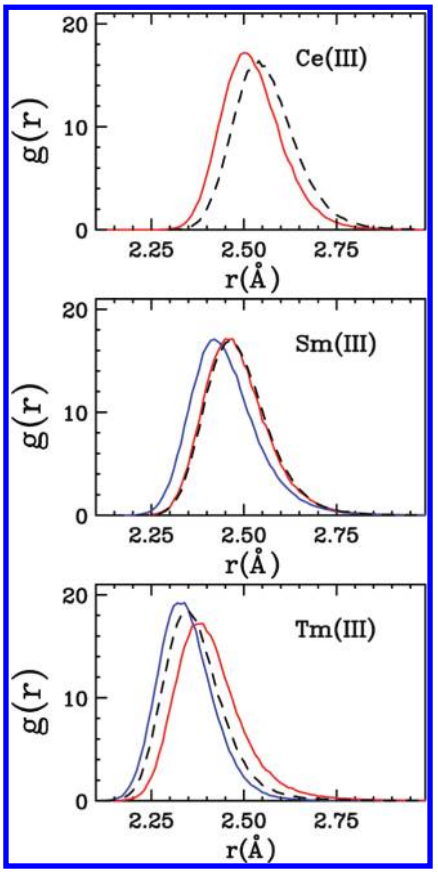

Figure 4. Ln(III)-O $g(r)$'s obtained from the MD simulations using the 9-fold Shannon radii (red line), 8-fold Shannon radii (blue line), and the new ionic radii (dashed black line).

constrained parameters. These conditions reduce meaningfully the indeterminacy on the structural parameters, namely, the average distance values of a nearest neighbor shell can be obtained with an accuracy of less than 0.01 Å while the error on the first shell coordination number is about 0.5. An exhaustive discussion on the effect of the Gaussian approximation on the accuracy on the structural parameters and a comparison with the results obtained with asymmetric peaks for Ln(III) ion aqueous solutions are reported in ref 30.

Table 2. Ionic Radii (Å) of Lanthanoid(III) Cations in Aqueous Solution and Crystal Ionic Radii Listed by Shannon for 8-Fold and 9-Fold Coordination

	IR_{new}[a]	IR_{Mar}[b]	IR_{Hey}[c]	IR_8[d]	IR_9[d]
La(III)	1.250	1.14	1.17	1.16	1.216
Ce(III)	1.220	1.16	1.13	1.143	1.196
Pr(III)	1.200	1.15	1.14	1.126	1.179
Nd(III)	1.175	1.08	1.14	1.109	1.163
Sm(III)	1.140	1.06	1.13	1.079	1.132
Eu(III)	1.120	1.06	1.08	1.066	1.120
Gd(III)	1.105	1.00	1.01	1.053	1.107
Tb(III)	1.090	1.01	1.00	1.040	1.095
Dy(III)	1.075	0.98	1.00	1.027	1.083
Ho(III)	1.055		0.99	1.015	1.072
Er(III)	1.040	0.97	0.99	1.004	1.062
Tm(III)	1.025	0.97	0.98	0.994	1.052
Yb(III)	1.010		0.91	0.985	1.042
Lu(III)	0.995	0.95	0.97	0.977	1.032

[a] This work. [b] Ref 2. [c] Ref 3. [d] Ref 1.

The difficulty in gathering experimental values for the ion−solvent distances with the appropriate accuracy is mainly responsible for the wide scatter in ionic radii present in the literature.[2,3] Different sets of ionic radii for Ln(III) ions in aqueous solution are plotted in Figure 3 together with the 8-fold and 9-fold Shannon radii. While a very regular behavior is observed for the crystal ionic radii, the values derived for aqueous solution by Marcus[2] and Heyrovska[3] show an unexpected up-and-down trend.

These findings have stimulated us to revise the lanthanoid ionic radii using more accurate Ln(III)-water distances obtained from a careful analysis of the EXAFS data. In particular, we used a single asymmetric shell to model the Ln(III) first hydration sphere. The Ln−O bond length is defined as the average distance of the distribution, and its value is highly correlated with the asymmetry of the function defined by the β parameter. For this reason we used the MD results to have a reliable model of the asymmetry of the systems, and the EXAFS minimizations were carried out forcing the β parameter to vary less than 5% from the MD values listed in Table 3. Note that the MD simulations used in this step have been carried out using the Shannon ionic radii and are completely independent from the EXAFS results. Moreover, while the Ln−O distances obtained from the MD simulations depend strongly on the ionic radii used in the potential, β is related both to the asymmetry of the hydration complexes and to the dynamical behavior of the system and is substantially independent of the choice of the ionic radii (see Figure 4). Use of β values obtained from MD simulations results in a constrained minimization of the EXAFS data that allowed us to enhance the accuracy of the refined structural parameters as compared to previous determinations.[5] A complete list of the structural parameters obtained from the EXAFS analysis is reported in Table 1.

Starting from these results we calculated a new set of ionic radii for Ln(III) ions in aqueous solution using eq 6 (see Table 2 and Figure 3). We adopted a R_{water} value of 1.350 Å that corresponds to the Shannon radius of a coordinated oxygen atom. The

dx.doi.org/10.1021/ic200260r |Inorg. Chem. 2011, 50, 4572–4579

Table 3. Ln−O First Shell Structural Parameters of Ln(III) Ions in Aqueous Solution Obtained from the MD Simulations Using the 8-Fold Shannon Ionic Radii, the 9-Fold Shannon Ionic Radii, and the New Ionic Radii[a]

	DM_{new}		$DM_{(8)}$		$DM_{(9)}$	
	R(Å)	β	R(Å)	β	R (Å)	β
La−O	2.585	0.47			2.540	0.47
Ce−O	2.565	0.48			2.530	0.48
Pr−O	2.540	0.49			2.520	0.50
Nd−O	2.520	0.50			2.510	0.51
Sm−O	2.490	0.52	2.450	0.54	2.480	0.51
Eu−O	2.475	0.55	2.440	0.57	2.475	0.55
Gd−O	2.460	0.59	2.425	0.60	2.470	0.58
Tb−O	2.445	0.61	2.410	0.62	2.460	0.60
Dy−O	2.430	0.64	2.390	0.62	2.450	0.64
Ho−O	2.415	0.65	2.370	0.62	2.435	0.64
Er−O	2.395	0.65	2.360	0.62	2.420	0.65
Tm−O	2.380	0.52	2.350	0.50	2.410	0.54
Yb−O	2.365	0.47	2.340	0.46	2.390	0.49
Lu−O	2.355	0.44	2.340	0.44	2.370	0.46

[a] R is the average distance of the Ln−O distribution, and β is the asymmetry parameter.

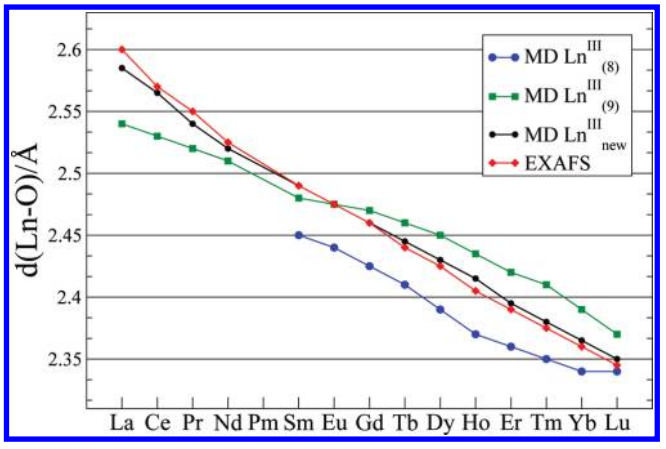

Figure 5. Mean Ln−O bond lengths of Ln(III) ions in aqueous solution obtained from the EXAFS experimental determination (red line) compared with those obtained from the MD simulations using the new ionic radii (black line), the 9-fold Shannon radii (green line), and the 8-fold Shannon radii (blue line).

motivations of this choice will be explained in Sec.3.2. The new ionic radii show a much more regular trend as compared to the previous determinations of Marcus and Heyrovska (see Figure 3).[2,3] As expected they decrease smoothly with increasing atomic number as a consequence of the lanthanoid contraction, and the slope is more pronounced as compared to the 9-fold and 8-fold Shannon radii. The reason for this behavior is the combination of two effects. First, the Ln−O average distance in solution is expected to be slightly longer than in the solid state because of the dynamical behavior of the system. In particular, a quite fast exchange takes place between the first and the second hydration shells that mainly involves the water molecules in the capping positions and shifts the average bond distance of the

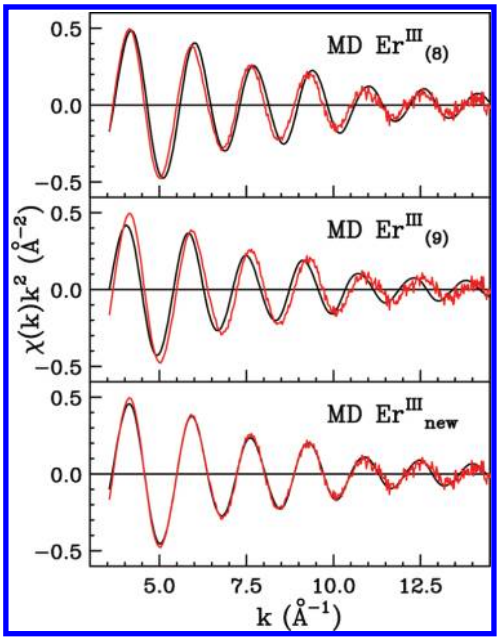

Figure 6. Comparison between the EXAFS experimental spectrum (red line) of Er(III) in aqueous solution and the $\chi(k)_{MD}$ theoretical signals (black line) calculated from the MD simulations using the 8-fold Shannon ionic radius (upper panel), the 9-fold Shannon ionic radius (middle panel), and the new ionic radius (lower panel).

Ln(III) hydration complexes toward longer values. Second, there is a smooth decrease of the hydration number across the series that shortens the Ln−O first shell average distances. As a result the new ionic radii are longer than the 9-fold Shannon ones for the lighter lanthanoid ions (La−Sm) that have an hydration number of about 9. For the heavier members of the series (Tb−Lu), where there is a smooth decrease of the hydration number, the new ionic radii are between the 9-fold and 8-fold Shannon ones. A last remark we would like to make concerns the choice of $d_{ion-water}$ used to determine the ionic radii. As previously mentioned we adopted the Ln−O average distances obtained from the EXAFS analysis that are 0.03 Å longer than the Ln−O $g(r)$ peak positions for all of the lanthanoid ions. Use of the peak position in the calculation would have resulted in a systematic decrease of the ionic radii of exactly 0.03 Å, while the trend would have been exactly the same.

3.2. Molecular Dynamics Simulations with New Ionic Radii. To test the reliability of these results we have carried out new MD simulations for all of the Ln(III) ions including the new ionic radii in the interaction potentials. The new B_{ij} and C_{ij} parameters are listed in Supporting Information, Table S1. To highlight the effect of the potential on the first hydration shell structure we report in Figure 4 the Ln−O $g(r)$'s obtained with different ionic radii for Ce(III), Sm(III), and Tm(III), as an example. The Ln−O average distances obtained from the different simulations show a significant shift while the shape of the distributions is unchanged.

A direct picture of the structural modifications occurring with the use of different potentials has been obtained by fitting the MD Ln−O $g(r)$'s with the gamma-like peaks of eq 1, and the best-fit parameters are listed in Table 3 and Supporting Information, Tables S2−S4. Figure 5 reports the Ln−O average distances obtained from all the MD simulations as a function of the lanthanoid atomic number, together with the EXAFS results. The

dx.doi.org/10.1021/ic200260r |Inorg. Chem. 2011, 50, 4572–4579

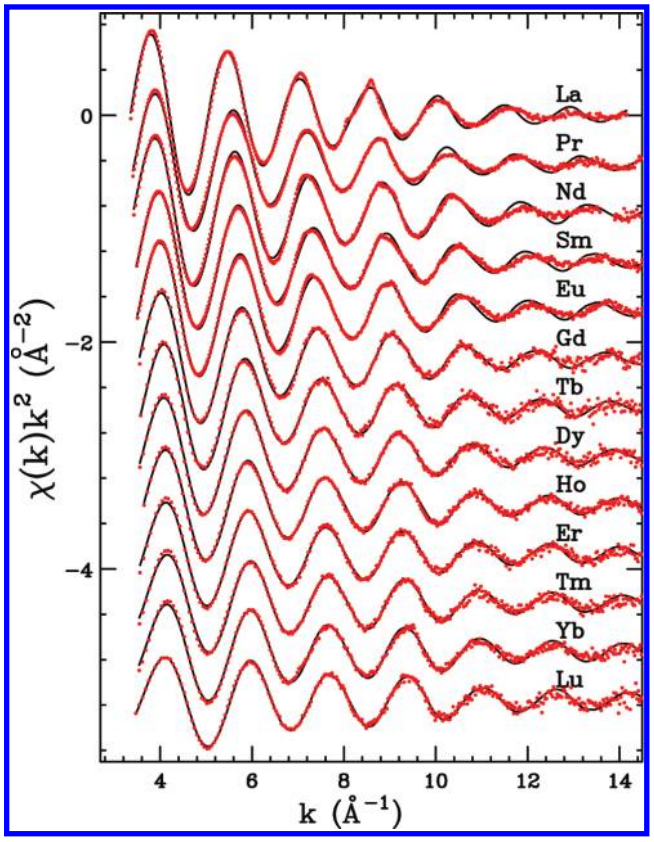

Figure 7. Comparison between the EXAFS experimental spectra of Ln(III) ions in aqueous solution (red dotted line) and the $\chi(k)_{MD}$ theoretical signals (black line) calculated from the MD simulations using the new ionic radii.

agreement between the experimental data and the MD simulations using the new ionic radii is excellent for all the elements of the series. Taking into account the picometer accuracy of the EXAFS technique in determining the first coordination shell distances, this result is a very strict test of the reliability of the new ionic radii. Inspection of Figure 5 reveals that, apart from the Eu(III) ion, an imperfect agreement exists between the Ln−O average distances obtained from the 9-fold and 8-fold MD simulations and the experimental determinations.

This finding has prompt us to define the water radius starting from the Eu(III) hydration geometry. For this element the MD simulation using the 9-fold Shannon ionic radius provides a theoretical determination of the Eu−O distance in perfect agreement with the EXAFS experimental result. This suggests that for this ion the lengthening of the ion−water distance associated with the dynamics of the solution is perfectly compensated by the decrease of the coordination number. As a result the 9-fold Shannon ionic radius coincides with the aqueous solution one, and this allowed us to determine R_{water} by subtracting from the experimental $d_{Eu-water}$ distance (2.470 Å) the Eu(III) 9-fold Shannon ionic radius (1.120 Å). The result is R_{water} = 1.350 Å that coincides with the Shannon ionic radius of a divalent oxygen atom. Note that this R_{water} value is in agreement with the previous determinations.[2,3,48]

As a last point, we would like to highlight the sensitivity of the EXAFS technique toward the structural changes of the Ln(III) hydration complexes obtained from the MD simulations using different ionic radii. To this end we calculated a theoretical signal $\chi(k)_{MD}$ by introducing in eq 2 the model $g(r)$'s obtained from the MD simulations. Direct comparison of the MD results with the EXAFS experiment data allows a better understanding of both the accuracy of the simulations and the sensitivity of the EXAFS technique.

The structural parameters derived from the MD simulations were kept fixed during the EXAFS analysis. In this way the first hydration shell structure obtained from the simulations can be directly compared with experimental data and the validity of the theoretical framework used in the simulations can be assessed. In Figure 6 the comparison between the EXAFS experimental signal of the Er(III) ion in aqueous solution and the $\chi(k)_{MD}$ theoretical curves calculated from the MD simulations using the 8-fold Shannon, 9-fold Shannon, and new ionic radii is reported. The $\chi(k)_{MD}$ signals are shown multiplied by k^2 for better visualization. For the MD simulations using the Shannon ionic radii there is a clear phase-shift between the experimental and the theoretical data. In particular the $\chi(k)_{MD}$ theoretical signals show a lower and higher frequency as compared to the experimental curve for the 8-fold and 9-fold MD simulations, respectively. This result proves that the Er−water mean distances obtained from the two simulations are respectively too short or too long as compared to the experiment. Conversely, a perfect agreement is obtained from the MD simulation using the new ionic radii. It is important to stress that we did not perform any refinement of the theoretical $\chi(k)_{MD}$ signal calculated from the MD data, because the non-structural parameters, and in particular E_0, were fixed to the values obtained from the previous analysis.

Finally, Figure 7 shows the comparison between the EXAFS experimental spectra and the $\chi(k)_{MD}$ calculated from the Ln−O and Ln−H $g(r)$'s obtained from the MD simulations using the new ionic radii for the entire series. In all cases the agreement between the theoretical EXAFS signal calculated from MD $g(r)$'s and the experiment is excellent, and this further proves the reliability of our results.

4. CONCLUDING REMARKS

In this work we have determined a new set of ionic radii in aqueous solution for the lanthanoid(III) ions. At variance with previous determinations, they show a very regular trend as expected for the Ln(III) series. The new ionic radii have been calculated starting from a very accurate determination of the Ln(III)−oxygen distance obtained from an improved analysis of the EXAFS experimental data. In particular, the EXAFS data analysis has been carried out using asymmetric peaks for the description of the cations hydration shells, and a reliable evaluation of the asymmetry of the distribution has been gained from MD simulations. This procedure allowed us to properly account for both the dynamical behavior of the system and the decrease of the hydration number across the Ln(III) series. The use of a "constrained" minimization in the EXAFS analysis increased the accuracy of the measured Ln−O distances as compared to previous experimental determinations, thus allowing us to determine ionic radii in solution with an accuracy comparable to that of the Shannon crystal ionic radii.

In conclusion, the original application of both experimental and computational techniques used in the present research paves the route for the systematic use of an integrated approach, with increased reliability, in the determination of cation and anion ionic radii in solution.

■ ASSOCIATED CONTENT

Supporting Information. Further details are given in Tables S1 to S4. This material is available free of charge via the Internet at http://pubs.acs.org.

■ AUTHOR INFORMATION

Corresponding Author
*E-mail: p.dangelo@caspur.it. Fax: +39-06-49913751.

■ ACKNOWLEDGMENT

This work was supported by CASPUR with the Standard HPC Grant 2010 entitled "A combined X-ray absorption spectroscopy, Molecular Dynamics simulations and Quantum Mechanics calculation procedure for the structural characterization of ill-defined systems". We acknowledge the European Synchrotron Radiation Facility for provision of synchrotron radiation facilities and GNR-Paris for partial funding.

■ REFERENCES

(1) Shannon, R. D. *Acta Crystallogr., Sect. A* **1976**, *32*, 751–767.
(2) Marcus, Y. *Chem. Rev.* **1988**, *88*, 1475–1498.
(3) Heyrovska, R. *Chem. Phys. Lett.* **2006**, *429*, 600–605.
(4) Helm, L.; Merbach, A. E. *J. Chem. Soc., Dalton Trans.* **2002**, 633–641.
(5) Persson, I.; D'Angelo, P.; De Panfilis, S.; Sandstrom, M.; Eriksson, L. *Chem.—Eur. J.* **2008**, *14*, 3056–3066.
(6) Duvail, M.; Souaille, M.; Spezia, R.; Cartailler, T.; Vitorge, P. *J. Chem. Phys.* **2007**, *127*, 034503.
(7) Duvail, M.; Spezia, R.; Vitorge, P. *ChemPhysChem.* **2008**, *9*, 693–696.
(8) Cossy, C.; Helm, L.; Merbach, A. E. *Inorg. Chem.* **1989**, *28*, 2699–2703.
(9) Helm, L.; Merbach, A. E. *Eur. J. Solid State Inorg. Chem.* **1991**, *28*, 245–250.
(10) Habenschuss, A.; Spedding, F. H. *J. Chem. Phys.* **1979**, *70* 2797–2806.
(11) Yamaguchi, T.; Nomura, M.; Wakita, H.; Ohtaki, H. *J. Chem. Phys.* **1988**, *89*, 5153–5159.
(12) D'Angelo, P.; Zitolo, A.; Migliorati, V.; Mancini, G.; Persson, I.; Chillemi, G. *Inorg. Chem.* **2009**, *48*, 10239.
(13) D'Angelo, P.; Zitolo, A.; Migliorati, V.; Persson, I. *Chem.—Eur. J.* **2010**, *16*, 684–692.
(14) Meier, W.; Bopp, P.; Probst, M. M.; Spohr, E.; Lin, J. L. *J. Phys. Chem.* **1990**, *94*, 4672–4682.
(15) Galera, S.; Lluch, J. M.; Oliva, A.; Bertran, J.; Foglia, F.; Helm, L.; Merbach, A. E. *New J. Chem.* **1993**, *17*, 773–9.
(16) Helm, L.; Foglia, F.; Kowall, T.; Merbach, A. E. *J. Phys.: Condens. Matter* **1994**, *6*, A132–A140.
(17) Kowall, T.; Foglia, F.; Helm, L.; Merbach, A. E. *J. Phys. Chem.* **1995**, *99*, 13078–13087.
(18) Chaussedent, S.; Monteil, A. *J. Chem. Phys.* **1996**, *105*, 6532–6537.
(19) Kowall, T.; Foglia, F.; Helm, L.; Merbach, A. E. *Chem.—Eur. J.* **1996**, *2*, 285–294.
(20) Kim, H.-S. *Chem. Phys. Lett.* **2000**, *330*, 570–576.
(21) Floris, F. M.; Tani, A. *J. Chem. Phys.* **2001**, *115*, 4750–4765.
(22) Chaumont, A.; Wipff, G. *Inorg. Chem.* **2004**, *43*, 5891–5901.
(23) Ikeda, T.; Hirata, M.; Kimura, T. *J. Chem. Phys.* **2005**, *122*, 244507.
(24) Clavaguéra, C.; Pollet, R.; Soudan, J. M.; Brenner, V.; Dognon, J. P. *J. Phys. Chem. B* **2005**, *109*, 7614–7616.
(25) Hughes, S. R.; Nguyen, T.-N.; Capobianco, J. A.; Peslherbe, G. H. *Int. J. Mass Spectrom.* **2005**, *241*, 283–294.
(26) Clavaguera, C.; Calvo, F.; Dognon, J.-P. *J. Chem. Phys.* **2006**, 124.
(27) Duvail, M.; Vitorge, P.; Spezia, R. *J. Chem. Phys.* **2009**, *130*, 104501.
(28) Duvail, M.; Vitorge, P.; Spezia, R. *Chem. Phys. Lett.* **2010**, *498*, 90–96.
(29) Filipponi, A.; Borowski, M.; Bowron, D. T.; Ansell, S.; De Panfilis, S.; Di Cicco, A.; Itiè, J.-P. *Rev. Sci. Instrum.* **2000**, *71*, 2422–2432.
(30) D'Angelo, P.; De Panfilis, S.; Filipponi, A.; Persson, I. *Chem.—Eur. J.* **2008**, *14*, 3045–3055.
(31) Filipponi, A.; Di Cicco, A. *Phys. Rev. B* **1995**, *52*, 15135–15149.
(32) Filipponi, A.; Di Cicco, A.; Natoli, C. R. *Phys. Rev. B* **1995**, *52*, 15122–15134.
(33) D'Angelo, P.; Barone, V.; Chillemi, G.; Sanna, N.; Mayer-Klauke, W.; Pavel, N. *J. Am. Chem. Soc.* **2002**, *124*, 1958–1967.
(34) Chillemi, G.; D'Angelo, P.; Pavel, N.; Sanna, N.; Barone, V. *J. Am. Chem. Soc.* **2002**, *124*, 1968–1976.
(35) Spezia, R.; Duvail, M.; Vitorge, P.; Cartailler, T.; Tortajada, J.; D'Angelo, P.; Gaigeot, M.-P. *J. Phys. Chem. A* **2006**, *110*, 13081–13088.
(36) D'Angelo, P.; Migliorati, V.; Guidoni, L. *Inorg. Chem.* **2010**, *49*, 4224–4231.
(37) Pham, V. T.; Tavernelli, I.; Milne, C. J.; van der Veen, R. M.; D'Angelo, P.; Bressler, C.; Chergui, M. *Chem. Phys.* **2010**, *371*, 24–29.
(38) Thole, B. T. *Chem. Phys.* **1981**, *59*, 341–350.
(39) *Handbook of Physics and Chemistry*; CRC Press: Boca Raton, FL, 1996.
(40) Jorgensen, W. L.; Chandrasekhar, J.; Madura, J. D.; Impey, R. W.; Klein, M. L. *J. Chem. Phys.* **1983**, *79*, 926–935.
(41) (a) Hutchinson, F.; Wilson, M.; Madden, P. A. *Mol. Phys.* **2001**, *99*, 811–824. (b) Okamoto, Y.; Suzuki, S.; Shiwaku, H.; Ikeda-Ohno, A.; Yaita, T.; Madden, P. A. *J. Phys. Chem. A* **2010**, *114*, 4664–4671.
(42) Salanne, M.; Simon, C.; Turq, P.; Madden, P. A. *J. Phys. Chem. B* **2008**, *112*, 1177–1183.
(43) Souaille, M.; Loirat, H.; Borgis, D.; Gaigeot, M.-P. *Comput. Phys. Commun.* **2009**, *180*, 276–301.
(44) Sprik, M. *J. Chem. Phys.* **1991**, *95*, 2283.
(45) Essmann, U.; Perera, L.; Berkowitz, M. L.; Darden, T.; Lee, H.; Pedersen, L. G. *J. Chem. Phys.* **1995**, *103*, 8577–8593.
(46) Duvail, M.; Spezia, R.; Cartailler, T.; Vitorge, P. *Chem. Phys. Lett.* **2007**, *448*, 41–45.
(47) Heyrovska, R. *Chem. Phys. Lett.* **1989**, *163*, 207–211.
(48) David, F.; Vokhmin, V.; Ionova, G. *J. Mol. Liq.* **2001**, *90*, 45–62.
(49) Ohtaki, H.; Radnai, T. *Chem. Rev.* **1993**, *93*, 1157–1204.
(50) D'Angelo, P.; Di Nola, A.; Mangoni, M.; Pavel, N. V. *J. Chem. Phys.* **1996**, *104*, 1779–1790.
(51) Roccatano, D.; Berendsen, H. J. C.; D'Angelo, P. *J. Chem. Phys.* **1996**, *108*, 9487–9497.
(52) D'Angelo, P.; Pavel, N. V. *J. Chem. Phys.* **1999**, *111*, 5107–5115.
(53) Mancini, G.; Sanna, N.; Barone, V.; Migliorati, V.; D'Angelo, P.; Chillemi, G. *J. Phys. Chem. B* **2008**, *112*, 4694–4702.
(54) Chillemi, G.; Mancini, G.; Sanna, N.; Barone, V.; Della Longa, S.; Benfatto, M.; Pavel, N. V.; D'Angelo, P. *J. Am. Chem. Soc.* **2007**, *129*, 5430–5436.
(55) D'Angelo, P.; Migliorati, V.; Mancini, G.; Chillemi, G. *J. Phys. Chem. A* **2008**, *112*, 11833–11841.